buildings

MDPI

Article

Experimental Study on the Propagation Law of Explosive Stress Wave in Cement Mortar with Weak Layers

Sanfeng Liu, Hansheng Geng, Xinli Kong, Yinzhi Zhou, Peng Wang * and Fengnian Jin *

State Key Laboratory for Disaster Prevention & Mitigation of Explosion & Impact, Army Engineering University of PLA, Nanjing 210007, China; liusanfeng008@163.com (S.L.); hsgeng@aeu.edu.cn (H.G.); xlk80@126.com (X.K.); zhouyinzhi_2009@yeah.net (Y.Z.)

* Correspondence: wp0608@163.com (P.W.); jinfn2009@163.com (F.J.)

Abstract: The weak layer has good attenuation performance when it comes to the explosive stress wave, which can be used in protective structures. In this paper, a cement mortar specimen was designed, cast, and tested. Under inner explosion, due to the expansion of air in the explosive hole, the tensile cracks formed around the explosive hole are mainly in a damage pattern. In ordinary cement mortar, the transmittance is decreasing as the distance increases. At a distance of 8 cm to 14 cm from the explosive center, the average transmittance is 50.16%, 12 cm to 18 cm, while the average transmittance is 62.89%, increasing by 12.73%. Adding one weak layer into the cement mortar, the transmittance of one weak layer is 43.37%. The effect of increasing weak layers in short spacing is not obvious, and the transmittance of the second and third weak layer is about 80%, much less than the first layer. The softer the weak layer and the larger the wave impedance, the smaller the transmission coefficient is. The research proves that the weak layer has excellent attenuation performance when it comes to the explosive stress wave.

Keywords: explosive stress wave; weak layer; transmittance; wave impedance

Citation: Liu, S.; Geng, H.; Kong, X.; Zhou, Y.; Wang, P.; Jin, F. Experimental Study on the Propagation Law of Explosive Stress Wave in Cement Mortar with Weak Layers. *Buildings* **2022**, *12*, 687. https://doi.org/10.3390/buildings12050687

Academic Editor: Łukasz Sadowski

Received: 6 April 2022
Accepted: 12 May 2022
Published: 20 May 2022

1. Introduction

Buildings are often under serious threat during explosions. For buildings, especially civil defense engineering buildings, the requirement of anti-explosion performance is getting higher and higher. Effectively improving the resistance to explosion is a current research hotspot in protective structures [1].

Many scholars have studied the concrete structural response under blast loading. Yuen et al. [2], Yao et al. [3], and Feng et al. [4] studied the response of a concrete plate subjected to blast loading, revealing the damage patterns of concrete plate under various scaled distances. The studies showed that flexibility and high strength can enhance the anti-explosion performance of the concrete plate. Wang et al. [5], Shi et al. [6], and Aoude et al. [7] investigated the dynamic behaviors of the concrete column and frame under blast loading, revealed interactions between the explosive shock wave and concrete column and frame, and improved the theoretical formula to predict the dynamic response of concrete columns. Song et al. [8] studied the elastic–plastic dynamic responses of arches subjected to blast loading, showing that the resistance of the arch can be increased by flexible supports. Fallah et al. [9] studied the P–I diagram of the elastic–plastic hardening and elastic–plastic softening single-degree-of-freedom model under blast loading, revealing that the blast energy per unit of maximum displacement increases as inverse ductility increases, or as the hardening index increases (softening index decreasing).

With the research on concrete structural dynamic response making progress, many scholars have begun to study the improvement of the structural anti-explosion performance. Improving concrete strength is a common way to improve the anti-explosion performance of the protective structure, such as adding fiber into the concrete. Nicolaides et al. [10], Jiao et al. [11], Kalman et al. [12], and Wu et al. [13] studied the dynamic performance of

fiber-reinforced cementitious composite. By studying the dynamic performance of fiber-reinforced concrete panels and cementitious composite-filled steel tubes experimentally, they revealed the anti-explosion performance of concrete with fibers.

With the advantages of a high-strength and low-elastic modulus, the fiber-reinforced polymer (FRP) has a good advantage in improving the anti-explosion performance of the concrete structure. Chen et al. [14] studied the dynamic performance infill walls retrofitted with carbon fiber-reinforced polymer bars (CFRP) subjected to blast loading. Mutalib et al. [15] investigated the failure of the FRP-reinforced concrete (RC) column. Lee et al. [16] and Liu et al. [17] evaluated the experimentally dynamic response and anti-explosion performance of the RC beam with FRP bars under blast loading. Through this research, with the addition of FRP, the dynamic displacement of the concrete structure increased. However, the concrete collapse decreased significantly, and the anti-explosion performance improved greatly. FRP have a wide application prospect in increasing the anti-explosion performance of the protective structure.

The elastic and weak protective layer can increase the ductility of the structure and reduce the explosive stress wave, and it is also an excellent protective measure. Many scholars focus on the research on the overall dynamic response of the structure with an elastic and weak protective layer. Fallon et al. [18], Bahei et al. [19], and Liu et al. [20] studied the dynamic response of the concrete structure with a weak layer on the impacted face, subjected to blast loading. Fatt et al. [21] researched the theoretically dynamic response of a polymer-retrofitted concrete brick wall subjected to blast loading. It is revealed that the weak layer has excellent anti-spalling ability and greatly increases the anti-explosion performance of the concrete structure, and the enclosed weak layer is the most efficient.

There is also some amount of research focused on the explosive stress wave attenuation of the weak layer in the concrete structure. Liu et al. [22] numerically studied the propagation law of the explosive stress wave in rock mass with a group of parallel filling joints and multiple small spacing filling joints. Pandya et al. [23] experimentally studied stress wave attenuation during ballistic impact for four types of polymer matrix composites. Wang et al. [24] experimentally studied stress wave attenuation characteristics in the multilayer weak layer. This research shows that the weak layer with different structures can clearly attenuate stress waves. Through theoretical analysis and fitting the experimental data, they acquired the mathematical characterization of stress waves attenuated by structures with different weak layers.

Previous studies have focused on the dynamic response of the concrete structure. In this research, an explosive experiment has been designed and implemented, and then calculated and analyzed based on the experimental data. The stress wave attenuation performance of the weak layer was evaluated quantificationally and subjected to explosive loading. Five kinds of cement mortar specimens (specimens A–E) were cast and studied experimentally. Specimens with weak layers were under inner explosion. Moreover, there were amounts of 2.0 g, 3.3 g, 4.3 g, and 5.5 g TNT explosives in this experiment. The propagation law and stress wave attenuation in the weak layer were studied, which enrich the research on concrete protective structure.

2. Explosive Experiment Design

2.1. Specimens

Five kinds of specimens were designed to study the stress wave attenuation law of the weak layer, as shown in Figure 1. Four specimens are square, specimens A–D, as shown in Figure 1. "E1" represents the incident pressure measurement point, and "E4" represents the transmission pressure measurement point. The distance between two measurement points is 6 cm. The dimensions are 30 cm × 30 cm × 20 cm. Specimen A did not have a weak layer. Specimen B has one weak layer, and the distance between the measurement point and the weak layer is 3 cm. Specimen C has two weak layers, and the distance between the measurement point and weak layer is 2 cm. Specimen D has three weak layers, and the distance between the measure point and weak layer is 1.5 cm, as listed in Table 1. The

specimens are made into layers and bonded with special glue. The weak layer is made up or 3 mm-thickness mica flakes. There is an explosive hole with a diameter of 4 cm. It is 6 cm away from the top and 13 cm away from the left side.

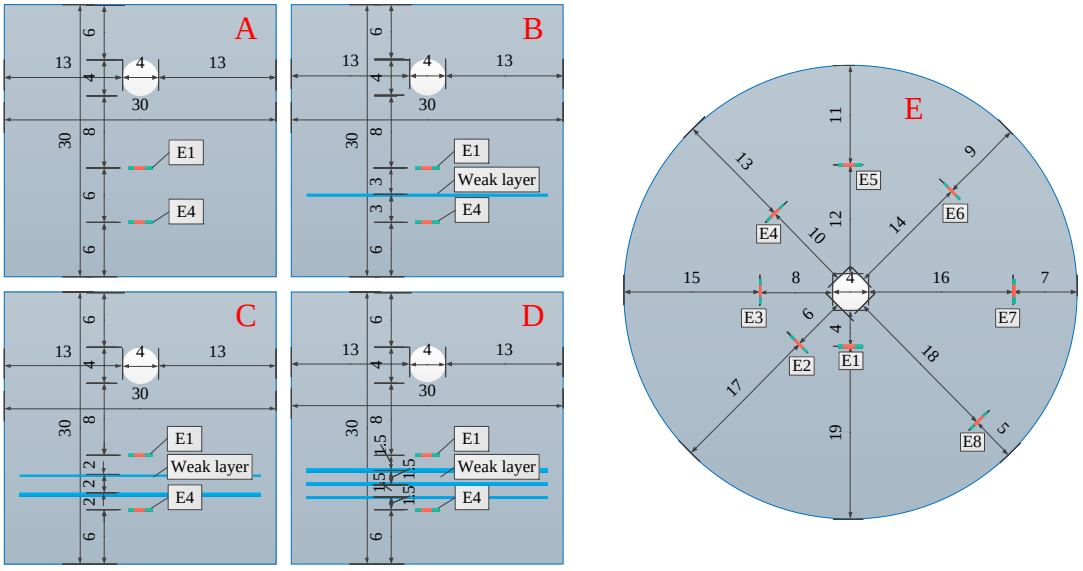

(**a**)

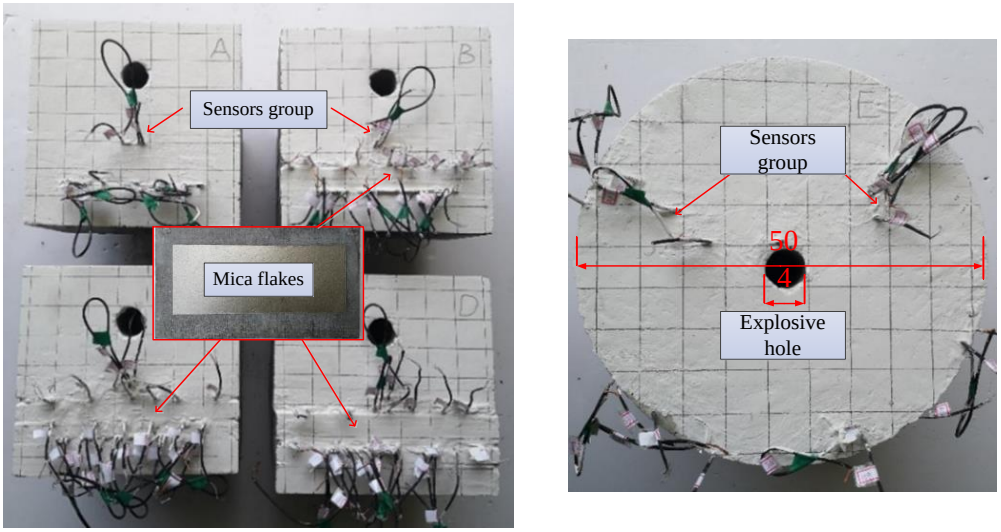

(**b**)

Figure 1. Specimens A–E of (**a**) design dimension and (**b**) Material object.

Table 1. TNT explosive of the specimens.

Specimens	A	B	C	D	E
Weak layer	0	1	2	3	0
Distance (cm)	-	3	2	1.5	-
TNT explosive (g)	-	0.5	-	-	0.5
	-	2.0	2.0	2.0	2.0
	-	3.3	3.3	3.3	3.3
	-	-	4.3	4.3	4.3
	5.5	-	-	-	5.5

One specimen is ordinary cylindrical without a weak layer, specimen E—the diameter is 25 cm and the height is 20 cm, as shown in Figure 1. It creates a cylindrical explosive

hole with a diameter of 4 cm and a length of 20 cm in the center, setting 8 groups of sensors to surround the explosive hole. A group of sensors includes one PVDF piezoelectric sensor and two strain gauges. The first group is 4 cm away from the explosive hole, and the angle is 90°. The distance between each group and the explosion center increases successively by 2 cm, and the angle of each group is increasing successively by 45°.

2.2. Materials Strength

In order to reduce the interference of the coarse aggregate of concrete on the propagation of the explosive stress wave, cement mortar replaced the concrete in this experiment. The polyurea, foamed concrete, and so on are the commonly used weak layer materials in explosions. A mica flake is composed of many minerals, and the wave impedance is low and has a certain strength, which has excellent attenuation performance when it comes to the explosive stress wave. To ensure that the weak layer is uniform and does not get damaged in the experiment, we selected mica flakes as the weak layer. The cement mortar was made in the laboratory according to the M40. The mass ratio of OPC (ordinary Portland cement) 42.5 cement, sand, water, and water reducer is 1:0.8182:0.1818:0.0061. The specimens are cured for 28 days in standard curing conditions. The uniaxial compressive strengths of the cement mortar specimen and the mica flake were tested, as shown in Figure 2. The dimensions of the cement mortar specimen are 70.7 mm × 70.7 mm × 70.7 mm. The uniaxial compressive strength of the cement mortar specimen is 36.35 MPa, as shown in Figure 2a. The diameter of mica flakes is 7.5 cm, and the height is 1 cm. The density of mica flakes is 2100 kg/m^3. It is obvious that the stress-strain curve of mica flakes is nonlinear, as shown in Figure 2b. With the stress increasing, the mica flakes deformation tends to be stable, and the curve gradually tends to a straight line. The Young's modulus is 0.149 GPa, calculated from the data of 4.5 MPa and 9 MPa. The average wave velocity of the ultrasonic longitudinal wave measured by the nonmetallic acoustic detector is 253 m/s.

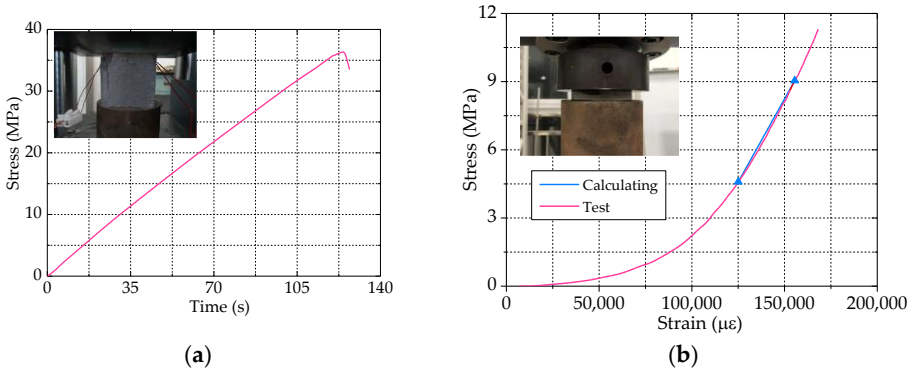

(**a**) (**b**)

Figure 2. The uniaxial compressive stress-strain curves of (**a**) the cement mortar and (**b**) mica flake.

2.3. Measure Technology

The PVDF piezoelectric sensor is widely used in measure vibration and pressure load. When the pressure is loaded on the sensor, it results in a corresponding resistance change, and an output signal is generated that is proportional to the pressure [25]. In this experiment, the PVDF piezoelectric sensor is connected to the DH8302 dynamic data acquisition system through a special charge conditioner, collecting the electric charge-time data. Both electric charge data and strain-time data have a linear relationship with the stress wave, so electric charge and strain are used to calculate the stress wave attenuation.

The sensors group and the data acquisition system are shown in Figure 3a. One PVDF piezoelectric sensor and two strain gauges are pasted on a prefabricated cement mortar block, the dimension is 4 cm × 4 cm × 0.5 cm, which was made by the same strength as the experiment specimen. Zhao et al. [26] found that setting a specimen close to the edge of the specimen can eliminate the influence of tensile waves on the edge. In this experiment, four

cement blocks were placed around the edges of the specimen to eliminate the influence of tensile stress waves at the specimen boundary.

The PVDF piezoelectric sensor is set in the middle, denoted by "E". Two strain gauges are bonded on the side, represented by "S". The measure points and the explosion devices are shown in Figure 3b. The distance between the first group of sensors and the explosion center is 10 cm, and the data of S1, E1, and S2 are used to represent incident explosive stress waves. The second to sixth group sensors are arranged from left to right. The distance between the second group of sensors and the right edge of the specimen is 1 cm, and each group of sensors is separated by 2 cm. The vertical depth of the explosion center is 16 cm. The data from the second to the sixth groups of sensors are used to represent the transmission of explosive stress waves. The thickness of the mica flakes is 3 mm, which is set in the middle of the sensors E1 and E4, keeping an equal distance between the incident point and transmission point.

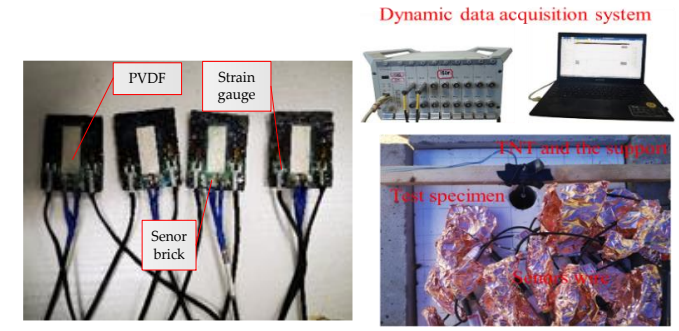

(**a**)

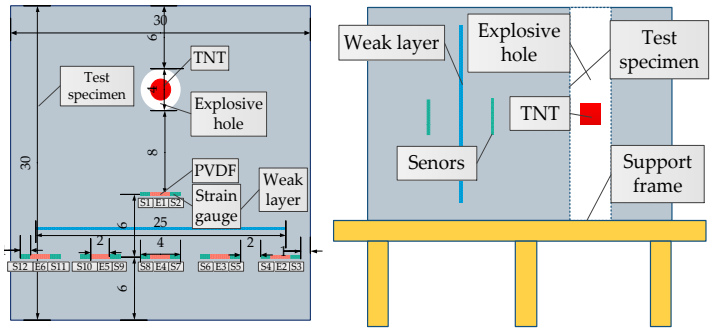

(**b**)

Figure 3. Explosion testing: (**a**) Sensors and measure system; (**b**) Sensor distributions.

2.4. Experiment Protocol

In the experiment, the specimens were placed on a steel frame. Installing the TNT explosive in the center of the explosive hole made sure that the explosive hole was not closed. The TNT explosive consists of a TNT mass block and an electric detonator. The electric detonator detonated the TNT mass block and is equivalent to a 0.5 g TNT mass block. The mass of the TNT explosive (including the TNT mass block and electric detonator) for each specimen is listed in Table 1. The normal explosive experiment at 2.0 g, 3.3 g, and 4.3 g TNT explosive, also added individually 0.5 g and 5.5 g TNT explosive according to experiment progress. The shape of the TNT explosive is a cylinder with a diameter of 10 mm, and the heights of the TNT explosives with different masses are different.

3. Damage Levels under Explosive Loading

The damage patterns of exploded specimens are shown in Figure 4. Moreover, a 0.5 g TNT explosive is used as a test to examine whether the dynamic data acquisition system is working or not. Specimen B and specimen E are completely elastic without any crack

or failure. At 2.0 g TNT explosive, due to the expansion of air in the explosive hole, the tensile cracks formed around the explosive hole. Three cracks formed in specimen B and specimen D, and the length is about 6 cm and the angles are 120° around the explosive hole. One crack formed in specimen C, the length is also about 6 cm, and no crack formed in specimen D.

At 3.3 g TNT explosive, the number of tensile cracks increased around the explosive hole. The top of specimens B–D is completely cracked, and the width is about 2 mm. The number of cracks increased to about 6, a transverse crack formed at the layer, and specimen C was damaged. With thicker concrete around the explosive hole, the overall tensile strength of specimen E is higher than that of specimen C and specimen D. Just one crack formed in specimen E—the length is about 4 cm.

At 4.3 g TNT explosive, specimen C and specimen D are completely blasted into four pieces. Six cracks formed in specimen E—two cracks about 25 cm, and three cracks about 5 cm. Damage levels are similar to specimen C and specimen D at 3.3 g TNT explosive.

At 5.5 g TNT explosive, specimen E is completely damaged and divided into three parts along the original cracks. In this experiment, the high compressive strength and low tensile strength of cement caused all the tensile damage in the specimen and no erosion damage. The same engineering design should pay more attention to the tensile of concrete.

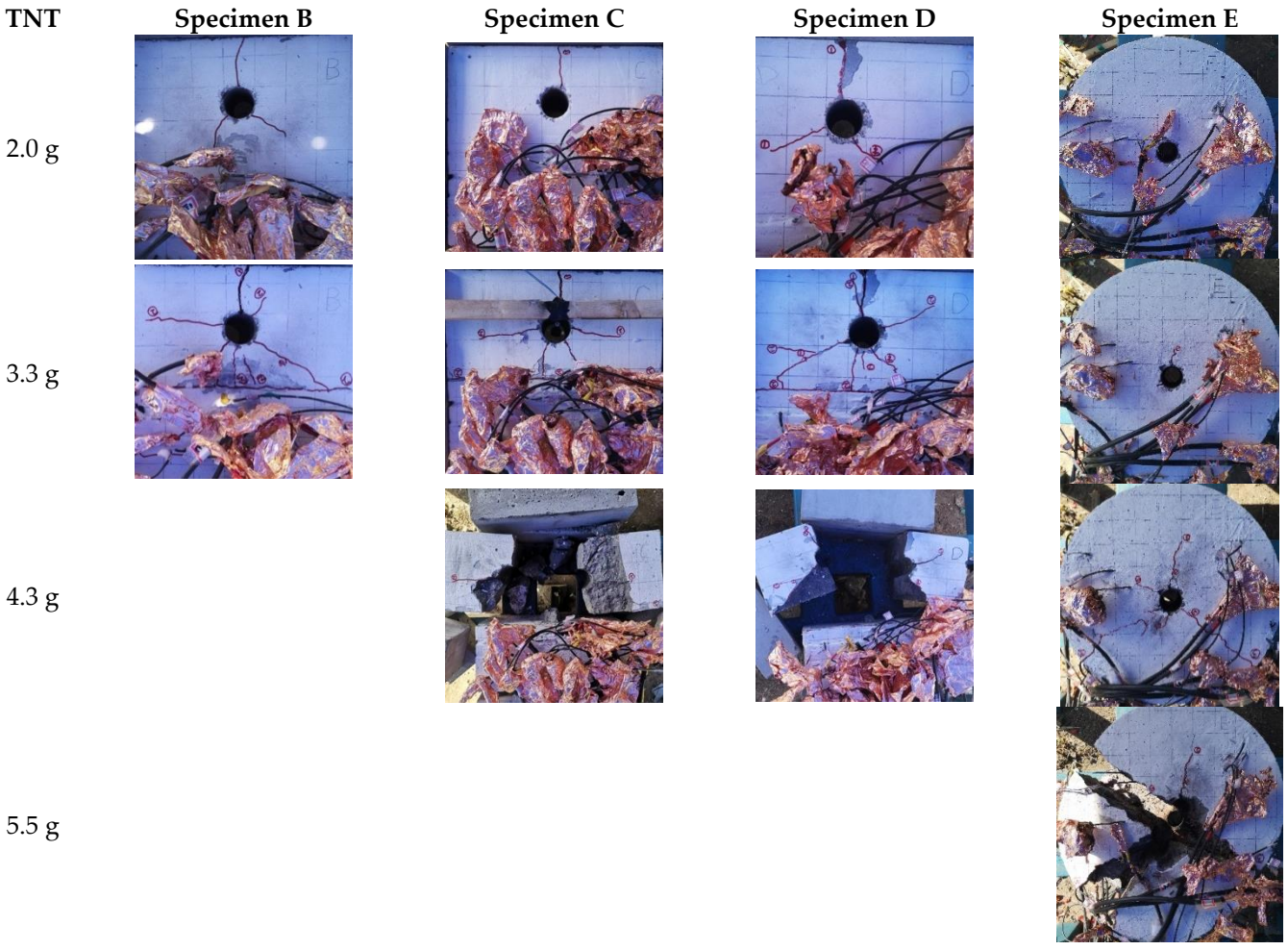

Figure 4. Damage patterns of exploded specimens with TNT mass increased from 2.0 g, 3.3 g, 4.3 g to 5.5 g.

4. Propagation Law of Explosive Stress Wave in Cement Mortar

4.1. Calculating with the Electric Charge

As a comparison, the attenuation of explosion stress wave in common cement mortar is studied. Specimen E is made of ordinary cement mortar specimen, and without a weak layer. Five explosive experiments are performed to study the attenuation of the stress wave in cement mortar. A total of 8 groups were made, and each includes one PVDF piezoelectric sensor and two strain gauges. The PVDF piezoelectric sensor is placed in the middle, denoted by "E". Two strain gauges bonded on the side, denoted by "S". S1, S2, and E1 form a group of sensors 6 cm away from the center of the explosion. S3, S4, and E2 form a group of sensors 8 cm away from the center of the explosion. The distance between each sensor and the explosion center is listed in Table 2.

Table 2. The distance between each sensor and the explosion center.

Distance (cm)	**6**	**8**	**10**	**12**	**14**	**16**	**18**	**20**
Electric charges	E1	E2	E3	E4	E5	E6	E7	E8
Strains	S1–S2	S3–S4	S5–S6	S7–S8	S9–S10	S11–S12	S13–S14	S15–S16

The range of the PVDF piezoelectric sensor is 100,000 pC; the measured electric charge signal is proportional to the explosive stress wave. In this experiment, the electric charge data represent the explosive stress wave data. The transmittance of stress waves in cement mortar is studied by comparing the peak value of the electric charge. The electric charge curves are shown in Figure 5, and the dashed lines represent out-of-range data. In fact, this experiment lasted three days—different specimens with different TNT explosives were at different times. To make it more intuitive, we determined the zero point of time according to the time in peak values of electric charge. The peak values of electric charge are listed in Table 3.

Table 3. Peak values of electric charge.

Electric Charge	**E1**	**E2**	**E3**	**E4**	**E5**	**E6**	**E7**	**E8**
Distance (cm)	6	8	10	12	14	16	18	20
0.5 g ($\times 10^3$ pC)	-	79.11	69.34	49.76	30.41	27.73	25.32	14.02
2.0 g ($\times 10^3$ pC)	-	94.28	82.56	54.56	58.34	34.09	37.25	25.88
3.3 g ($\times 10^3$ pC)	-	-	91.47	34.66	62.7	53.08	35.13	30.85
4.3 g ($\times 10^3$ pC)	-	95.8	-	57.84	-	59.62	40.21	50.59
5.5 g ($\times 10^3$ pC)	-	-	-	58.44	59.98	36.94	-	20.95

Removing out-of-range data and using the peak values of electric charge to calculate the average transmittance at each distance. Define the transmittance of stress wave in 6 cm cement mortar T_3:

$$T_{n-2} = \frac{E_n}{E_2} \times 100\%, (n = 5, 6, 7, 8) \quad (1)$$

where T_{n-2} represents the transmittance of stress wave E_n to E_2. The same calculate mode in other distances and measure points.

Former Soviet Union scientists combined theory and experiment, and obtained the stress wave attenuation equation of spherical explosive in rock, which is the widely accepted:

$$\sigma_r = -\frac{p}{\widetilde{r}^{\alpha}} \quad (2)$$

where α represents stress attenuation coefficient, p is the initial pressure. $\widetilde{r} = r/r_0$, r is the distance between the measurement point to the explosive center; r_0 is the radius of the explosive hole. α is an attenuation index, thus calculated:

$$\alpha = 2 - \frac{\mu}{1-\mu} \tag{3}$$

where μ is the Poisson's ratio of rock, 0.25 is selected, here.

According to equations of stress wave propagation in spherical and cylindrical charge packs in completely elastic media, the stress wave attenuation equation of cylindrical explosive in rock can produce:

$$\sigma_r = -\frac{p}{\widetilde{r}^{\frac{\alpha}{2}}} \tag{4}$$

According to the above equation, Zhang [27] derived and modified the equation of the stress wave attenuation of the cylindrical charge in rock:

$$\sigma_r = -\frac{p}{\widetilde{r}^{\beta}} \tag{5}$$

where $\beta = \frac{\alpha}{2}K_1$, according to formerly abundant of experiment, 1.05 to 1.15 is advised to K_1. In this research, 1.1 is selected.

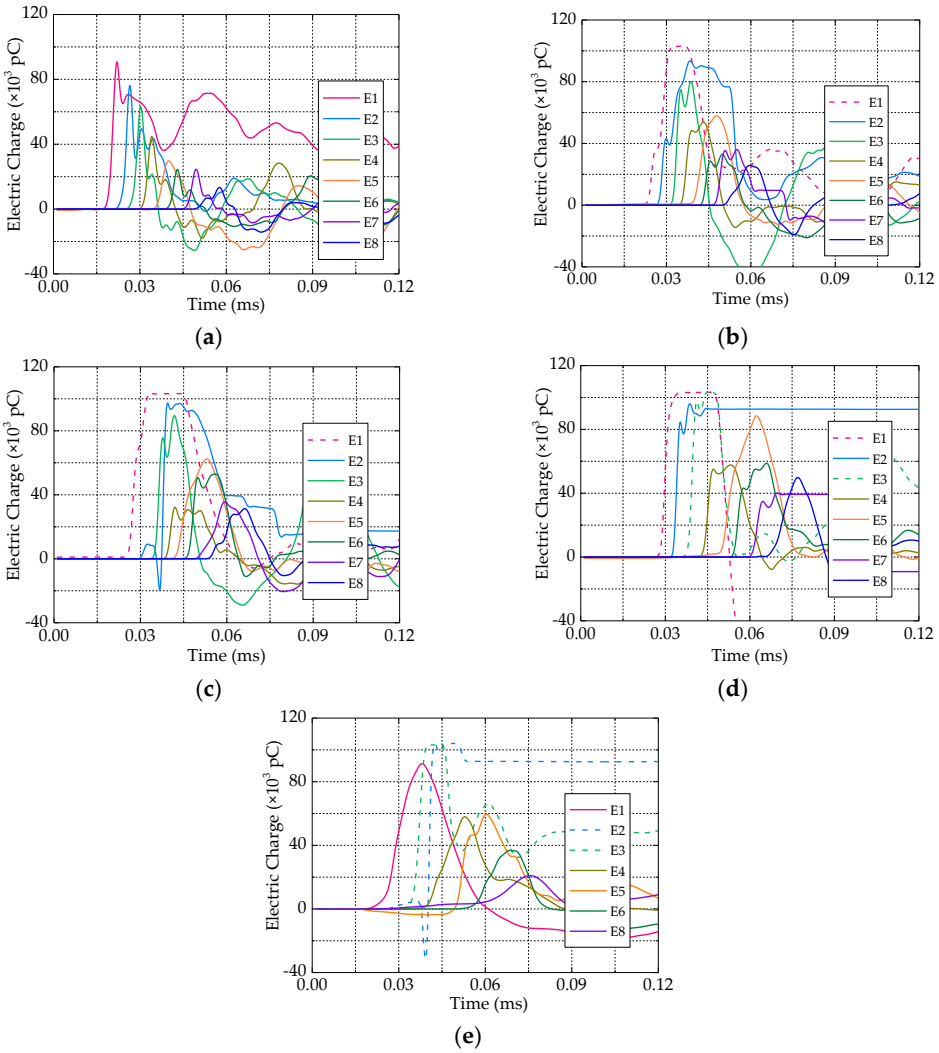

Figure 5. The electric charge curves of specimen E under explosion of (**a**) 0.5 g TNT, (**b**) 2.0 g TNT, (**c**) 3.3 g TNT, (**d**) 4.3 g TNT, and (**e**) 5.5 g TNT.

The transmittance in each distance and measure point is calculated by the experimental data and theoretical equation which are shown in Figure 6 and Table 4. The transmittances of E2 and E4 are calculated by the experimental data are closed to that by the theoretical

equation, which is reliable. The distance between E2 and E5 is 6 cm, and the average transmittance is 50.16%. The same distance is found between E4 and E7, while the average transmittance is 62.89%, increasing to 12.73%. The two points are further away from the explosive center, the greater the transmittance is.

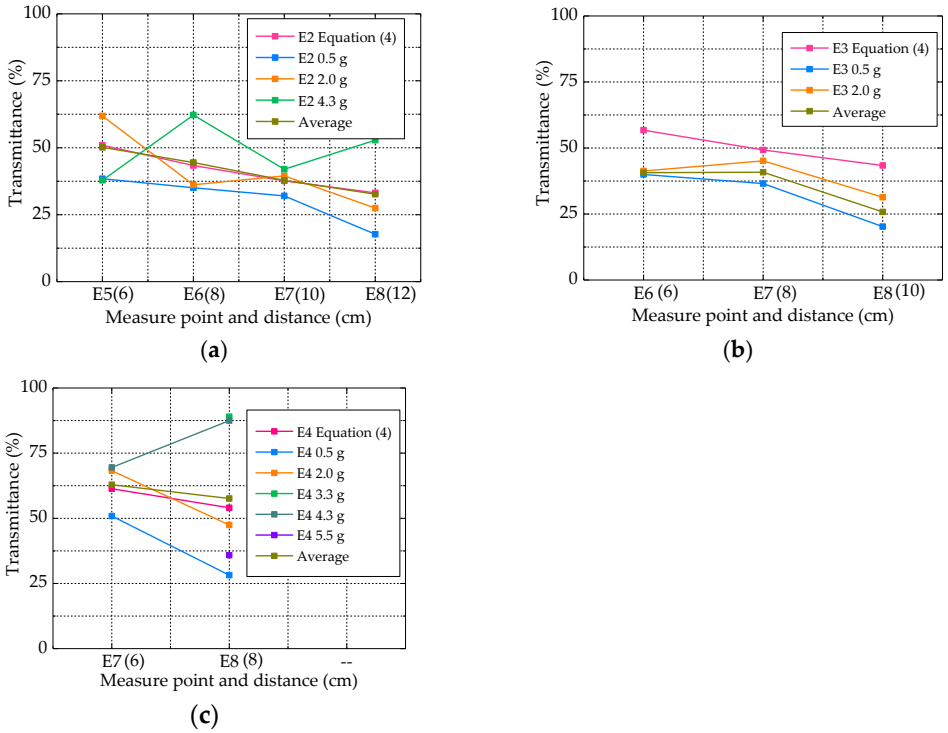

Figure 6. Transmittance in each distance in (**a**) E2 measure point, (**b**) E3 measure point, and (**c**) E4 measure point.

Table 4. Transmittance in each distance and measure point.

Incident Point	**E2**				**E3**			**E4**	
Transmission point	E5	E6	E7	E8	E6	E7	E8	E7	E8
Distance (cm)	6	8	10	12	6	8	10	6	8
Equation (4) (%)	54.07	46.69	41.02	36.53	59.66	52.42	46.69	64.05	57.04
0.5 g (%)	38.44	35.05	32.01	17.72	39.99	36.52	20.22	50.88	28.18
2.0 g (%)	61.88	36.16	39.51	27.45	41.29	45.12	31.35	68.27	47.43
3.3 g (%)	-	-	-	-	-	-	-	-	89.01
4.3 g (%)	-	62.23	41.97	52.81	-	-	-	69.52	87.47
5.5 g (%)	-	-	-	-	-	-	-	-	35.85
Average (%)	50.16	44.48	37.83	32.66	40.64	40.82	25.78	62.89	57.59

4.2. Calculating with the Strain

Due to the impact of the explosive stress wave, some strain gauges were damaged. The typical strain curves are shown in Figure 7, and the peak values of strain are listed in Table 5. At 3.3 g TNT explosive, the maximum strains of S5 and S6 are 685 με and 705 με, respectively. The peak strains of S11 and S12 are 387 με and 307 με, respectively. The average transmittance calculated with the peak values of strain at distances of 6 cm is 52.68%. The average transmittance calculated with the peak values of strain at distances of 8 cm is 39.60%, as listed in Table 6. The stress wave transmittance and attenuation rate in cement mortar are calculated from the peak values of strains, and the values are closed to that calculated from E2 electric charges.

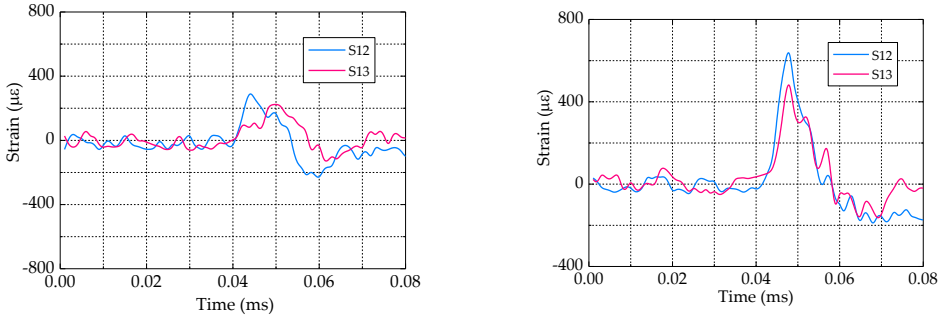

Figure 7. Typical strain curves of specimen E under explosion of (**a**) 0.5 g TNT and (**b**) 2.0 g TNT.

Table 5. Peak values of strains.

Strain	S5 (με)	S6 (με)	S11 (με)	S12 (με)	S13 (με)
0.5 g	685	705	381	307	224
2.0 g	1210	-	1172	676	518
3.3 g	1435	-	1475	-	628

Table 6. Transmittance and attenuation rate.

Distance (cm)	6	8	10	12
Transmittance (%)	52.68	39.60	-	-

5. Propagation Law of Stress Wave in Weak Layer

5.1. Calculating with the Electric Charge

The typical electric charge curves of specimen A to D are shown in Figure 8, and the peak values of electric charge and transmittance are listed in Table 7. The distance between E1 and E4 is 6 cm. Specimen A is made of ordinary cement mortar without a weak layer. At 5.5 g TNT explosive, the peak value of electric charge at E1 is 94.23 × 103 pC, and E4 is 53.18 × 103 pC, as listed in Table 7. Define average transmittance of explosive stress wave in 6 cm cement mortar T_A:

$$T_A = \frac{E_4}{E_1} \times 100\% \tag{6}$$

where $E1$ and $E4$ are the peak value of electric charge.

Defining the relative transmittance, which is calculated with respect to sample A, the relative transmittance of one weak layer T_{AB}:

$$T_{AB} = \frac{T_B}{T_A} \times 100\% \tag{7}$$

where T_A and T_B is the transmittance of specimens A and B, respectively.

The transmittance of the explosive stress wave between E1 and E4 in specimen A is 56.44%. The transmittance in 6 cm ordinary cement mortar, away 10 cm to 16 cm from the explosive center, is shown in Table 8. As the transmittance calculated by electric charge from specimen E is less than Equation (4) and other experimental results, as shown in Table 4, we choose the transmittance calculated by Equation (4), 59.66%. The average transmittance is 56.26%, calculated by the transmittance of specimen E and specimen A. Specimen B has one weak layer. Since at 3.3 g TNT explosive, specimen B is damaged and in the data measured exist errors, only the explosions of 0.5 g and 2.0 g are considered. At 0.5 g TNT explosive, the peak value of electric charge at E1 is 68.59 × 103 pC, and E4 is 16.79 × 103 pC, as shown in Figure 8b. Calculating with the experimental data, the transmittance of the explosive stress wave between E1 and E4 in specimen B is 24.48%. The transmittance of one weak layer is 43.37% compared to the non-weak layer.

Specimen C has two weak layers, and at 4.3 g TNT explosive, specimen B is completely damaged—only the data of 2.0 g and 3.3 g are effective. At 2.0 g TNT explosive, the peak value of electric charge at E1 is 98.33 × 103 pC, and E4 is 20.25 × 103 pC, as shown in Figure 8c. The transmittance of specimen C is 20.59%. Compared to the non-weak layer, the transmittance of two weak layers is 36.49%. When compared to one weak layer, the transmittance of two weak layers is 84.11%.

Specimen D has three weak layers. At 2.0 g TNT explosive and 3.3 g TNT explosive, E1 was out-of-range. At 4.3 g TNT explosive, the failure of the specimen made the explosive stress wave that enters E1 less than that at 2.0 g TNT explosive. The peak value of electric charge at E1 is 69.51 × 103 pC, while E4 is 11.51 × 103 pC, as shown in Figure 8d. The transmittance of specimen D is 16.56%. Compared to the non-weak layer, specimen D, the transmittance of three weak layers is 29.34%. Meanwhile, compared to two weak layers, the transmittance of three weak layers is 80.42%. The results show that the transmittance of the explosive stress wave by the second and third weak layers does not decrease obviously. This experiment further verifies that the transmittance of the explosive stress wave through the weak layer is not decreased obviously when the distance between weak layers is small.

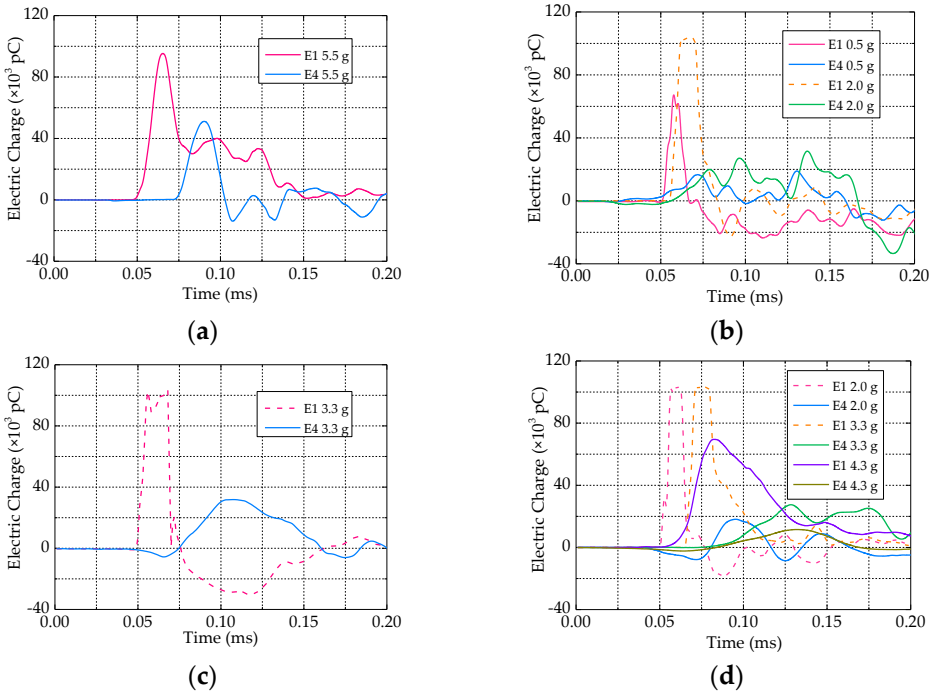

Figure 8. Typical electric charge curves of (**a**) specimen A, (**b**) specimen B, (**c**) specimen C, and (**d**) specimen D.

Table 7. Peak values of electric charge and transmittance.

Specimen	E1 (×10³ pC)	E4 (×10³ pC)	Transmittance (%)	Relative Transmittance (%)
A (5.5 g)	94.23	53.18	56.44	-
B (0.5 g)	68.59	16.79	24.48	43.37
C (2.0 g)	98.33	20.25	20.59	36.49
D (4.3 g)	69.51	11.51	16.56	29.34

Table 8. Transmittance of 6 cm ordinary cement mortar.

Transmittance (%)	Electric Charge from Specimen E	Strain from Specimen E	Electric Charge from Specimen A	Strain from Specimen A	Average
Ordinary cement mortar	59.66	52.68	56.44	-	56.26

5.2. Calculating with the Strain

We select the data of four measurement points S6 to S9, which are in the middle of specimen. Typical strain curves are shown in Figure 9, the peak values of strain and transmittance is shown is Table 9. The peak values of strain and transmittance at 2.0 g and 3.0 g TNT explosive are listed in Table 8. At 5.5 g TNT explosive, the peak value of S6 in specimen A is 303 με, and S7 is 306 με.

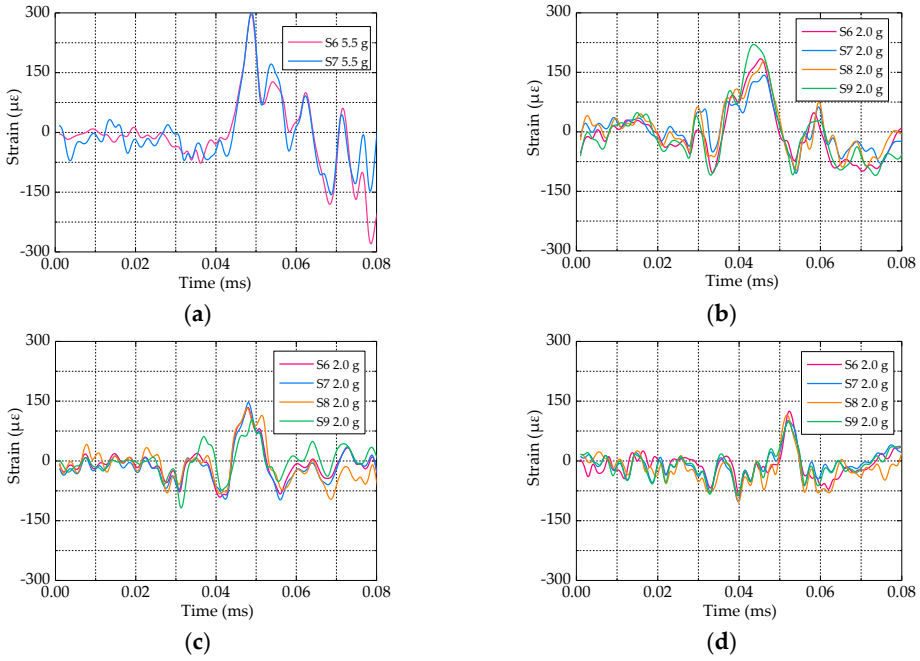

Figure 9. Typical strain curves of (**a**) specimen A, (**b**) specimen B, (**c**) specimen C, and (**d**) specimen D.

Table 9. Peak values of strain and transmittance.

TNT	Specimen	S6 (με)	S7 (με)	S8 (με)	S9 (με)	Relative Transmittance (%)
2.0 g	B	186	148	186	209	-
	C	128	149	162	144	79.97
	D	136	110	124	110	75.58
3.3 g	B	219	234	264	239	-
	C	167	209	-	189	78.80
	D	122	135	140	125	69.29

For specimen B, at 2.0 g TNT explosive, the peak value of S6 to S9 is about 180 με. At 3.3 g TNT explosive, the peak value of S6 to S9 is about 230 με. The relative transmittance of the second weak layer is calculated with the strain data of specimen B and specimen C. The average relative transmittance of the second weak layer is 79.39%. The average relative of the third weak layer is 72.44%. The average transmittance is calculated with electric charges and strains, as shown in Table 10. The average transmittances of the second and weak third layers are 80.97% and 70.84%, respectively. Once again, it is proven that the

transmittance of explosive stress wave through the weak layer is not decreased obviously when the distance between the weak layers is small.

Table 10. Transmittance of weak layers.

Transmittance (%)	One Weak Layer	Two Weak Layers	Second Weak Layer	Three Weak Layers	Third Weak Layer
electric charge from specimen A–D	43.37	36.49	84.14	29.34	67.65
Strain from specimen A–D	-	-	79.97 78.80	-	75.58 69.29
Average	43.37	36.49	80.97	29.34	70.84

The results calculated with electric charges and strains show that the average transmittance of explosive stress wave in 6 cm ordinary cement mortar, 12 cm to 18 cm away from the explosive center, is 57.34%. The transmittance of one weak layer is 43.37%. This happens in the multi-weak layer, when the layers are close to each other. The transmittance mainly decreased by the first weak layer. The transmittance of two weak layers is 36.49%. The transmittance of three weak layers is 29.34%. The average transmittances of the second and weak third layers are not obvious, which are 80.97% and 70.84%, respectively.

6. Theoretical Analysis Transmission and Reflection of Explosive Stress Wave

6.1. Doubles-Layer Materials

Fang et al. [28] have researched the transmission and reflection of explosive stress waves in different materials. When an explosion stress wave encounters the interface of two different materials, the explosion stress wave causes the transmission stress wave in other materials. At the same time, reflected stress waves can also be generated in the original material. According to the interface boundary conditions, the numerical relationship along the incident stress wave, the reflected stress wave and transmitted stress waves are established:

$$P_{1i} + P_{1f} = P_{2j} \tag{8}$$

$$V_{1i} + V_{1f} = V_{2j} \tag{9}$$

where P and V are the pressure and particle velocity of the stress wave, respectively; 1 and 2 represent the first layer material and the second layer material; i, f, and j represent the incident, the reflected and transmitted stress wave, respectively. Then, the reflection coefficient, F, and the transmission coefficient, T:

$$F = \frac{1-n}{1+n} \tag{10}$$

$$T = \frac{2}{1+n} \tag{11}$$

where $n = \frac{\rho_1 c_1}{\rho_2 c_2} = Q_1/Q_2$, ρ is density of the elastic media; c is the velocity of the stress wave; ρc is the material wave impedance, Q. n is the ratio of material wave impedances in the interface. As shown in Figure 10, it is clearly shown that the softer the second layer of material, and the larger the wave impedance, the smaller the transmission coefficient.

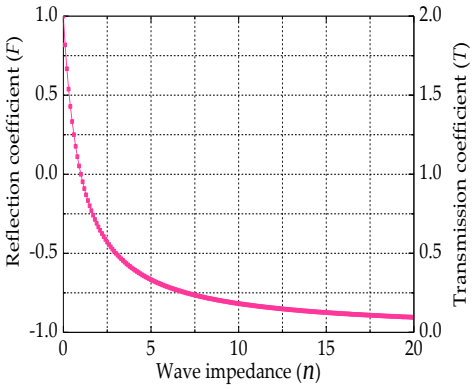

Figure 10. Relationship among F, T and n.

6.2. Three-Layer Materials

The propagation of the explosive stress wave in three-layer materials is shown in Figure 11. It is assumed that material 1 and material 3 are thick enough. Neither the surface of material 1 nor the bottom surface of material 3 are considered. An explosive shock wave is transmitted from material 1 to the interface at time $t = 0$, the transmission stress peak values of material 3:

$$P_{31i} = T_{3i}P_{21i} = T_{3i}T_{2i}P_{1i} \tag{12}$$

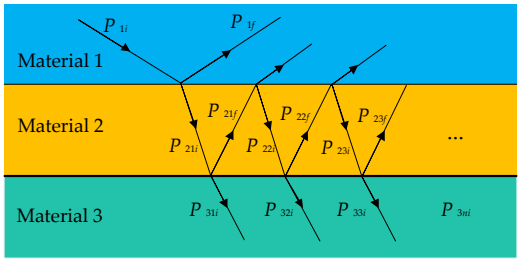

Figure 11. The transmission route of a stress wave in a three-layered material.

The peak value of transmission stress that enters material 3 after reflection is:

$$P_{32i} = T_{3i}P_{22i} = T_{3i}F_{2f}^{1}P_{21f} = T_{3i}F_{2f}^{1}F_{2f}P_{21i} = T_{3i}F_{2f}^{1}F_{2f}T_{2i}P_{1i} \tag{13}$$

$$P_{33i} = T_{3i}(F_{2f}^{1}F_{2f})^{2}T_{2i}P_{1i} \tag{14}$$

$$P_{3ni} = T_{3i}(F_{2f}^{1}F_{2f})^{n-1}T_{2i}P_{1i} \tag{15}$$

where:P_{31i}, P_{32i} and P_{3ni} are the peak values of transmission stress waves entering material 3, respectively. P_{1i} is the peak value of the incident stress wave; P_{21i} is the peak value of transmission stress wave from material 1 to material 2; P_{21f}, P_{22f}, P_{2nf} are the peak values of reflected stress waves from material 2 to material 3 in sequence; T_{2i} and T_{3i} are the transmission coefficients of stress wave propagation from material 1 to material 2 and from material 2 to material 3, respectively. F_{2f}^{1} and F_{2f} are the reflection coefficients from material 2 to material 1 and from material 2 to material 3, respectively.

Then, the sum of transmission stress peaks in material 3 is:

$$P_{3i} = \sum_{k=1}^{n_1} P_{3ki} = T_{3i}T_{2i}P_{1i}\frac{\left[1-\left(F_{2f}^{1}F_{2f}\right)^{n_1-1}\right]}{1-F_{2f}^{1}F_{2f}} \tag{16}$$

The sum of transmission stress peaks through fourth layers:

$$P_{4i} = \sum_{k=1}^{n_1} P_{4ki} = T_{4i}T_{3i}T_{2i}P_{1i}\frac{\left[1-\left(F_{2f}^{1}F_{2f}\right)^{n_1-1}\right]}{1-F_{2f}^{1}F_{2f}}\frac{\left[1-\left(F_{3f}^{1}F_{3f}\right)^{n_1-1}\right]}{1-F_{3f}^{1}F_{3f}} \tag{17}$$

T_{4i} is the transmission coefficients of stress wave propagation from the third layer material to the fourth layer material. F_{3f}^{1}, F_{3f} are the reflection coefficients from the third layer of material to the second layer of material and from the third layer of material to the fourth layer of material, respectively.

Propagating through a multilayer material, an explosive shock wave becomes a stress wave with a rise time. A multi-layer material can effectively reduce the peak value of an explosive stress wave, reducing the damage to the structure.

Fang et al. [28] studied the propagation of the multilayer material, but not considering the thickness of the layers. Li [29] improved the equivalent wave impedance method, in which layer thickness is considered, based on the continuous conditions of stress and velocity.

When the weak layer (material 2) thickness is d, the wave impedance is Q_1, the wave impedance of material 1 is Q_0. When the stress waves travel vertically to material 2, the equivalent wave impedance of material 2 is:

$$Y = \frac{Q_0\cos\delta_1 + \mathrm{i}Q_1\sin\delta_1}{\cos\delta_1 + \mathrm{i}(Q_0/Q_1)\sin\delta_1} \tag{18}$$

where i is imaginary, $\delta_1 = 2\pi h/\lambda_1$, λ_1 is the wave length; $\lambda_1 = Tv = v/f$, v is the wave velocity, f is the frequency.

Transmission and reflection coefficients T and R:

$$T = \frac{2Y}{Q_0+Y} = \frac{2[1+\mathrm{i}(Q_1/Q_0)\tan\delta_1]}{2+\mathrm{i}(Q_1/Q_0+Q_0/Q_1)\tan\delta_1} \tag{19}$$

$$R = \frac{Q_0-Y}{Q_0+Y} = -\frac{\mathrm{i}(Q_1/Q_0+Q_0/Q_1)\tan\delta_1}{2+\mathrm{i}(Q_1/Q_0+Q_0/Q_1)\tan\delta_1} \tag{20}$$

The amplitude:

$$|T|^2 = \frac{2Y}{Q_0+Y} = \frac{4\left[1+(Q_1/Q_0)^2\tan^2\delta_1\right]}{4+(Q_1/Q_0+Q_0/Q_1)^2\tan^2\delta_1} \tag{21}$$

$$|R|^2 = \frac{Q_0-Y}{Q_0+Y} = \frac{[(Q_1/Q_0+Q_0/Q_1)\tan\delta_1]^2}{4+[(Q_1/Q_0+Q_0/Q_1)\tan\delta_1]^2} \tag{22}$$

According to the experimental data, the explosion stress wave is simplified to a triangular load, the amplitude is 1, and the time τ is 25 microseconds, as shown in Figure 11a. The calculated transmission of the explosive stress wave through the weak layer expands the triangular load according to the Fourier series:

$$\delta_1(t) = \frac{2}{\pi}(\sin\frac{\pi}{\tau}t + \frac{1}{2}\sin\frac{2\pi}{\tau}t + \frac{1}{3}\sin\frac{3\pi}{\tau}t + \frac{1}{4}\sin\frac{4\pi}{\tau}t + ...), 0 \le t \le \tau \tag{23}$$

The general form of the Fourier series:

$$\delta_1(t) = \sum_{k=1}^{n_2} a_k \sin w_k t \tag{24}$$

The stress wave transmits the weak layer:

$$\delta_T(t) = \sum_{k=1}^{n_2} [T(wk) a_k \sin w_k t] \tag{25}$$

When there are ten reflections and refractions between layer materials, $n_1 = 10$. Li [29] confirmed $n_2 > 20$; the transmission is accurate. According to Li [29], layer thickness is considered, but just considering one weak layer. In this research, we considered the thickness and multilayer weak layers with Fang et al. [28] and Li [29], $n_2 = 35$. The explosive stress wave transmits the weak layer, as shown in Figure 12b. The transmissions of one weak layer, two weak layers, and three weak layers are 39.05%, 28.40%, and 21.50%, respectively. The experimentally calculated transmissions are 43.37%, 36.49%, and 29.34%, respectively, which are closed to theoretical values.

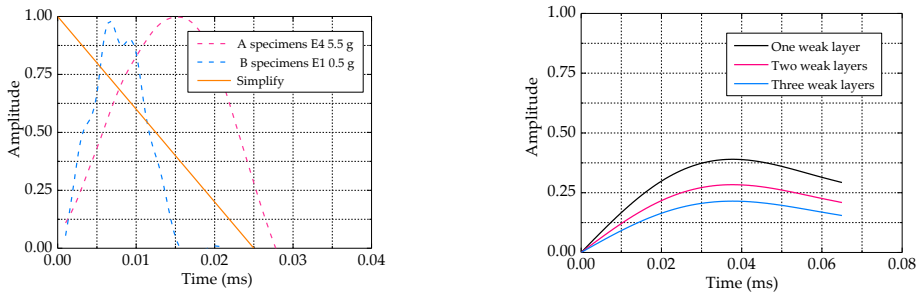

Figure 12. (**a**) The simplified explosion stress wave and (**b**) Transmission.

7. Conclusions

In this research, the propagation of the stress wave in multi-layer material is analyzed theoretically, and the propagation law of the explosive stress wave in cement mortar with the weak layer is studied experimentally. It is concluded that:

1. Through the multi-layer material, an explosive shock wave becomes a stress wave with a rise time. Multi-layer material can effectively reduce the peak value of explosive stress waves. Therefore, the damage to the structure can be weakened.
2. Moreover, 8 cm to 14 cm away from the explosive center, the average transmittance is 50.16%. Furthermore, for 12 cm to 18 cm, the average transmittance is 62.89%, increasing by 12.73%. The two points are further away from the explosive center, the greater the transmittance is.
3. The weak layer has good attenuation performance when it comes to the explosive stress wave, and the transmittance of one weak layer is 43.37%. When several weak layers are close to each other, there are reflections and refractions between layers. The transmittance mainly decreased in the first weak layer. The transmittances reduced by the second and the third weak layer are not obvious, that is, about 80.97% and 70.84%, respectively.
4. The experimental research proves that the weak layer has excellent attenuation performance when it comes to the explosive stress wave, and can be a choice in protective structures.

Author Contributions: Conceptualization, S.L. and H.G.; methodology, S.L. and H.G.; validation, S.L. and P.W.; resources, X.K.; data curation, X.K.; writing—original draft preparation, S.L.; writing—review and editing, Y.Z.; supervision and funding acquisition, F.J. All authors have read and agreed to the published version of the manuscript.

Funding: This research was funded by Natural Science Foundation of Jiangsu Province of China (BK20190572, BK20190573) and Science and Technology Project of Jiangsu Province of China (BE2020716). This support is gratefully acknowledged. The opinions and conclusions presented in this paper are those of the authors and do not necessarily reflect the views of the sponsoring organizations.

Conflicts of Interest: The authors declare no conflict of interest.

References

1. Yang, F.; Feng, W.H.; Liu, F.; Jing, L.; Yuan, B.; Chen, D. Experimental and numerical study of rubber concrete slabs with steel reinforcement under close-in blast loading. *Constr. Build. Mater.* **2019**, *198*, 423–436. [CrossRef]
2. Yuen, S.; Nurick, G.N. Experimental and numerical studies on the response of quadrangular stiffened plates. Part I: Subjected to uniform blast load. *Int. J. Impact. Eng.* **2005**, *31*, 55–83. [CrossRef]
3. Yao, S.J.; Zhang, D.; Chen, X.G.; Lu, F.Y.; Wang, W. Experimental and numerical study on the dynamic response of RC slabs under blast loading. *Eng. Fail Anal.* **2016**, *66*, 120–129. [CrossRef]
4. Feng, J.; Zhou, Y.Z.; Wang, P.; Wang, B.; Zhou, J.N.; Chen, H.L.; Fan, H.L.; Jin, F.N. Experimental research on blast-resistance of one-way concrete slabs reinforced by BFRP bars under close-in explosion. *Eng Struct.* **2017**, *150*, 550–561. [CrossRef]
5. Wang, X.G.; Ge, N.; Wang, C.M.; Su, Y.P. Research on simplified rc frame column model under blast load. *Adv. Mat. Res.* **2011**, *163–167*, 4346–4349. [CrossRef]
6. Shi, Y.C.; Hao, H.; Li, Z.X. Numerical simulation of blast wave interaction with structure columns. *Shock Waves* **2007**, *17*, 113–133. [CrossRef]
7. Aoude, H.; Dagenais, F.P.; Burrell, R.P.; Saatcioglu, M. Behavior of ultra-high performance fiber reinforced concrete columns under blast loading. *Int. J. Impact Eng.* **2015**, *80*, 185–202. [CrossRef]
8. Song, C.M.; Wang, M.Y.; Wang, D.R. Analysis of dynamic responses of arches with flexible supports subjected to blast loads. *Acta Armamentarii* **2008**, *29*, 813–818. (In Chinese)
9. Fallah, A.S.; Louca, L.A. Pressure–impulse diagrams for elastic-plastic-hardening and softening single-degree-of-freedom models subjected to blast loading. *Int. J. Impact Eng.* **2007**, *34*, 823–842. [CrossRef]
10. Nicolaides, D.; Kanellopoulos, A.; Petrou, M.; Savva, P.; Mina, A. Development of a new ultra high performance fibre reinforced cementitious composite (UHPFRCC) for impact and blast protection of structures. *Constr. Build. Mater.* **2015**, *95*, 667–674. [CrossRef]
11. Jiao, C.J.; Sun, W.; Gao, P.Z. Study on steel fiber reinforced high strength concrete subject to blast loading. *Eng. Mech.* **2008**, *25*, 158–166.
12. Kalman, D. Use of steel fiber reinforced concrete for blast resistant design. Master's Thesis, Kansas state university, Manhattan, KA, USA, 2010.
13. Wu, H.; Peng, Y.L.; Fang, Q. Experimental and numerical study of ultra-high performance cementitious composites filled steel tube (UHPCC-FST) subjected to close-range explosion. *Int. J. Impact. Eng.* **2020**, *141*, 103569. [CrossRef]
14. Chen, L.; Fang, Q.; Fan, J.Y.; Hao, H.; Liu, J. Responses of masonry infill walls retrofitted with CFRP, steel wire mesh and laminated bars to blast loadings. *Adv. Struct. Eng.* **2014**, *17*, 817–836. [CrossRef]
15. Mutalib, A.A.; Tawil, N.M.; Baharom, S.; Abedini, M. Failure Probabilities of FRP Strengthened RC Column to Blast Loads. *J. Teknol.* **2013**, *65*, 135–141. [CrossRef]
16. Lee, J.Y.; Jang, D.E.; Kwon, K.Y.; Yoon, Y.S. Evaluation of local damages and residual performance of blast damaged rc beams strengthened with steel fiber and FRP sheet. *J. Korea Concr. Inst.* **2014**, *26*, 627–634. [CrossRef]
17. Liu, S.F.; Zhou, Y.Z.; Zhou, J.N.; Zhang, B.; Jin, F.N.; Zheng, Q.; Fan, H.L. Blast responses of concrete beams reinforced with GFRP bars: Experimental research and equivalent static analysis. *Compos. Struct.* **2019**, *226*, 111271. [CrossRef]
18. Fallon, C.; Mcshane, G.J. Impact damage protection mechanisms for elastomer-coated concrete. *Int. J. Prot. Struct.* **2021**, *12*, 2128447695. [CrossRef]
19. Bahei, Y.A.; Dvorak, G.J. Behavior of sandwich plates reinforced with polyurethane/polyurea interlayers under blast loads. *J. Sandw. Struct. Mater.* **2007**, *9*, 261–281. [CrossRef]
20. Liu, Y.; Wang, P.; Jin, F.; He, H.G.; Fan, H.L. Blast responses of polyurea-coated concrete arches. *Arch. Civ. Mech. Eng.* **2021**, *21*, 30. [CrossRef]
21. Fatt, M.; Ouyang, X.; Dinan, R.J. blast response of walls retrofitted with elastomer coatings. *Mater. Struct.* **2004**, *15*, 129–138.
22. Liu, T.T.; Li, X.P.; Li, H.B.; Li, J.C.; Luo, Y. Numerical study on stress wave propagation across filled joints. *Chin. J. Rock Mech. Rock Eng.* **2016**, *35*, 3552–3560. (In Chinese)
23. Pandya, K.S.; Dharmane, L.; Pothnis, J.R.; Ravikumar, G.; Naik, N.K. Stress wave attenuation in composites during ballistic impact. *Polym. Test.* **2012**, *31*, 261–266. [CrossRef]
24. Wang, D.R.; Liu, J.Q.; Zhao, J.Y.; Li, H.J. Experimental Investigation on Stress Wave Attenuation in Multilayer Membrane Material. *J. Exp. Mech.* **2015**, *30*, 0401–0406. (In Chinese)
25. Fan, Z.Q.; Ma, H.H.; Shen, Z.W.; Lin, M.J. Stress Attenuation Mechanism of Foam Core Sandwich Panels Subjected to Close-Range Blast Loading. *Adv. Mat. Res.* **2014**, *945–949*, 561–566. [CrossRef]
26. Zhao, Y.T.; Hu, K.; Liu, S.L.; Kou, W.X. Cratering effect for a contact explosion at the joint of concrete structures. *J. Vib. Shock.* **2021**, *40*, 245–251.
27. Zhang, J.H. Study on the Attenuati on Law of Explosion Stress Wave in Rockof Cylinder Charge. Master's Thesis, North University of China, Taiyuan, China, 2005. (In Chinese).
28. Fang, Q.; Liu, J.C. *Underground Protection Structure*, 1st ed.; China Water&Power Press: Beijing, China, 2010; pp. 77–83.
29. Li, X.B. *Rock Dynamics Fundamentals and Applications*, 1st ed.; Science Press: Beijing, China, 2014; pp. 360–363.